Detecting Cirrus-Overlapping-Water Clouds and Retrieving Their Optical Properties Using MODIS Data

Fu-Lung Chang [(1)], Zhanqing Li [(1,2)]

(1) Earth System Science Interdisciplinary Center

(2) Department of Meteorology

University of Maryland, College Park, Maryland 20742

3 June 2004

Corresponding author: Dr. F.-L. Chang, Earth System Science Interdisciplinary Center, 2207 Computer and Space Sciences Bldg, University of Maryland, College Park, MD 20742.

Email: fchang@essic.umd.edu

Abstract

The ubiquitous presence of cirrus cloud overlapping low cloud poses a major challenge for retrieving cloud properties from weather satellites. This paper presents a novel retrieval algorithm that takes full advantage of the satellite data from the Moderate Resolution Imaging Spectroradiometer (MODIS). The main objectives are detecting cirrus-overlapping-low clouds, determining their optical depths and cloud-top altitudes, separately for the cirrus cloud and its underlying low cloud, and determining the emissivity for semi-transparent cirrus clouds. The overlapping clouds are identified using the MODIS cloud-top product estimated from the CO_2-slicing channel and infrared radiances from the 11μm channel. After an overlapped cirrus-above-water cloud is detected, initial estimates of cloud optical depths are first made from the 11-μm infrared and 0.65-μm visible channels for cirrus and water clouds, respectively. An automated iterative procedure follows by adjusting the cloud optical depths until computed radiances from the dual-layer model match with observed radiances from both channels. Cloud physical height is determined by the CO_2-slicing technique for the cirrus cloud and from neighboring water cloud pixels for the low cloud. A preliminary validation was conducted using cloud vertical structure inferred from ground-based radar and lidar data. The new algorithm is also compared with the traditional single-layer algorithm operationally used in the International Satellite Cloud Climatology Project (ISCCP) and the MODIS standard algorithm. It is shown that the assumption of a single cloud layer can cause systematic biases in cloud vertical distributions and optical properties. ISCCP tends to treat overlapped clouds as low clouds, whereas MODIS treats overlapped clouds as high cloud only, and the retrieved optical depths are biased positively or negatively depending if an ice or a water cloud model is adopted. The biases can be removed or lessened considerably by using the new algorithm applied to MODIS data.

1. Introduction

Multilayer clouds have been the most challenging cloud type for passive satellite remote sensing techniques developed so far. Cirrus clouds overlapping water clouds are the most often observed configuration of multi-layer cloud, as reported by surface observers and aircraft observations (Hahn et al. 1982, 1984; Warren et al. 1985; Tian and Curry 1989). For example, Hahn et al. (1982) used a 12-year record (1965-1976) of ship-reported synoptic observations over the North Atlantic Ocean to show that the probability of the coexistence of stratus cloud and cirrus cloud was often greater than 50% in the region between 30°N and 60°N. Tian and Curry (1989) analyzed the Air Force Global Weather Central 3-dimensional nephanalysis (Fye 1978) data during January 1979 over the North Atlantic Ocean between 40°N and 60°N and found that the probability of stratus cloud coexisting with cirrus cloud was about 61%. None of these data provided cloud optical depth and cloud-top height information, which is important for understanding the Earth's radiation budget and computing the heating rate of the atmosphere.

Detection of overlapped clouds and the retrieval of their optical properties can be achieved from a combination of ground-based active sensors like radar and lidar (Mace et al. 1997, 2001; Clothiaux et al. 2000; Wang and Sassen 2002). Using the 94-GHz radar reflectivity data observed at State College, Pennsylvania, Mace et al. (1997) found a similar probability (51%) of cirrus clouds occurring in conjunction with low clouds. Unfortunately, such ground-based remote sensing data are only available from a very small number of stations around the world. The longest continuous record of observations of cloud vertical structure has been made at the three major sites of the Atmospheric Radiation Measurement (ARM) Program (Ackerman and Stokes 2003). Given the high probability of occurrence of overlapping high and low clouds

and the difficulty in observing this cloud configuration from the ground on a global basis, satellite observation techniques offer the best means of tackling the challenge of identifying and determining the optical properties of such clouds.

Different methods have been proposed to detect multilayer clouds using passive remote sensing data. Baum et al. (1995) used the CO_2-slicing technique applied to the High resolution Infrared Radiation Sounder (HIRS) data to determine cirrus cloud heights. The spatial coherence technique (Coakley and Bretherton 1982) was applied to the Advanced Very High Resolution Radiometer (AVHRR) data to determine low cloud heights. Ou et al. (1996) presented a threshold test scheme to distinguish AVHRR pixels that contain non-overlapped low and high clouds and overlapped clouds. Baum and Spinhirne (2000) used a bispectral method on Moderate Resolution Imaging Spectroradiometer (MODIS) Airborne Simulator (MAS) 1.6-μm and 11-μm data to identify areas containing overlapped clouds. All of these methods were focused on the detection of overlapped clouds and not on the retrieval of cloud optical depth. Also, none has been applied over extensive areas or over long time periods. Other algorithms made use of a combination of microwave, visible and infrared measurements (Sheu et al. 1997; Lin et al. 1998; Ho et al. 2003), but were restricted to high thick clouds over ocean only.

Global cloud climatologies over both ocean and land have been generated using data from the International Satellite Cloud Climatology Project (ISCCP; Rossow and Schiffer 1999) and the MODIS (King et al. 2003; Platnick et al. 2003). The ISCCP scheme relies essentially on one infrared channel (~11 μm) to retrieve cloud-top height and one visible channel (~0.6 μm) to retrieve cloud optical depth both channels are common to all weather satellite sensors. Because cirrus clouds are mostly semitransparent at infrared wavelengths, the measured brightness temperatures are usually warmer than the ambient temperatures of the cirrus clouds, but colder

than the water clouds. Consequently, using this channel alone would place the cloud-top height between the two layers. To account for the cirrus emissivity, ann attempt was made to improve the retrieval of cirrus cloud-top heights using optical depths retrieved from the visible channel (Rossow and Schiffer 1999). This may alleviate the problem somewhat but cannot solve it due to fundamental limits in the information content. For thin cirrus clouds overlapping thick water clouds, the lower clouds overwhelm the signal in the visible channel.

For MODIS, cirrus cloud-top heights are retrieved using the partially absorbing multispectral infrared channels near the 15-μm CO_2 absorption bands; this retrieval scheme is known as the CO_2-slicing technique. The MODIS cloud optical depth is retrieved from different channels for different surface types, i.e. 0.65 μm over land, 0.86 μm over ocean, and 1.24 μm for ice/snow surface (Platnick et al. 2003). The CO_2-slicing technique was applied previously to the HIRS data (e.g., Menzel et al. 1992; Baum and Wielicki 1994). Similar to other retrieval methods, the standard CO_2-slicing technique assumes a single-layer cloud. Given a satellite's viewpoint from space, clouds highest in the atmosphere are preferentially detected. Thus, the majority of low clouds underlying high clouds are often obscured and neglected. Since the CO_2-slicing method is very sensitive to clouds at the highest altitude, a high thick cloud would be identified based on the retrieved optical depth.

The best tool to deal with the problem is space-borne cloud radar such as the CloudSat, scheduled for launch in 2005 (Stephens et al. 2002). Because this sensor provides a single nadir point of view, it will take time to amass enough samples to develop a meaningful global climatology of cloud vertical structure. Maximal exploitation of the conventional passive imaging sensors is thus highly desirable, which motivated this investigation. A more useful approach would be the combination of passively acquired data from MODIS with active radar

data from CloudSat. This can be achieved because the two sensors will follow one another in the same orbit; a merged cloud product will be developed by the CloudSat team (Stephens, private communication).

By virtue of the multi-spectral channels available from MODIS, we developed an algorithm that first identifies overlapped clouds on a pixel-level basis, and then determines the optical depths and heights of each individual cloud layer. The method can overcome some of the aforementioned limitations, as demonstrated using ground-based measurements from active remote sensors (Clothiaux et al. 2000; Mace et al. 2001) obtained at the ARM Southern Great Plains (SGP) site in north-central Oklahoma. Also, the method is versatile and fast enough for global application (Chang and Li 2004).

The paper is presented in the following order. Section 2 describes the retrieval algorithm. Section 3 presents the retrieval applications, sensitivity tests, and evaluations against ground-based retrievals and the current MODIS and ISCCP algorithms. Concluding remarks are given in Section 4.

2. Detection of Overlapped Clouds

Our algorithm is conceptually similar to that of Baum et al. (1995), but technically differs in many aspects. To identify multilayer cirrus cloud systems, Baum et al. (1995) applied the CO_2-slicing technique to the HIRS data for determining the cirrus cloud-top altitudes and their infrared effective emissivities. They then developed a fuzzy logic technique using AVHRR data to discriminate between single-layer high or low clouds and multi-layer clouds. Their method is

applicable to an array of pixels, but not to individual pixels, and does not retrieve cloud optical depth.

Our cirrus cloud-top altitude is also determined from the CO_2-slicing retrieval. Our low cloud-top altitude is inferred from the average of low cloud-top altitudes identified in neighboring pixels. Overlapping clouds are identified by the difference between the cloud-top temperature as determined from the CO_2-slicing channel and the brightness temperature from the 11-μm channel. If there are no adjacent pixels identified with low cloud, a representative mean low cloud-top altitude is determined from a larger neighboring area of ±125 km. If no low clouds are detected within the ±125-km area, the retrieval does not proceed. This could miss about 4% (absolute frequency of occurrence) of overlapped cirrus and water clouds on average around the globe (Chang and Li, 2004).

Figure 1 shows an example of the Terra/MODIS images of (a) 11-μm brightness temperature (K), (b) CO_2-slicing-retrieved cloud-top temperature, Tc, (K), and (c) 0.65-μm retrieved cloud optical depth. Note that the temperature data shown in Fig. 1b were estimated from cloud-top pressure using the atmospheric temperature and pressure profiles generated by the National Oceanic and Atmospheric Administration's (NOAA) National Centers for Environmental Prediction (NCEP) Global Data Assimilation System (Derber et al. 1991). Theparameters shown in the figure were retrieved by the MODIS single-layer cloud retrieval algorithm (Menzel et al. 2002), which was applied to MODIS radiance data acquired at 1715 UTC on April 2, 2001. The figure shows a geographical area of ~500 km × 300 km over the ARM SGP region in north-central Oklahoma. The entire scene is mostly overcast.

The CO_2-slicing technique is effective in detecting mid- to high clouds, including thin cirrus (Menzel et al. 1992; Wylie et al. 1994; Jin et al. 1996). This is clearly demonstrated in Fig. 1b. Nearly half of the image exhibits high cold clouds in contrast to the other half showing low warm clouds. The CO_2-slicing algorithm uses the ratios from four of the MODIS infrared channels (nominally at 13.34, 13.64, 13.94, and 14.24 μm) around the 15-μm CO_2 absorption band. They were designed together with other MODIS infrared channels to retrieve the profile of atmospheric temperature as well (Menzel and Gumley 2002).

The CO_2-slicing Tc represents the ambient temperature near the top of the highest cloud seen from space, while the 11-μm brightness Tc represents the bulk infrared emission, which is dictated by both cloud-top height and optical depth. Note that the brightness temperature is not a physical cloud temperature, but a simple transformation of thermal radiance into temperature. Figure 2 shows the comparisons of the two Tc and 0.65-μm cloud optical depth taken from the area within the square box (~ 50 x 50 km, centered on the ARM SGP Central Facility) shown in Fig. 1. From Fig. 2a, about 50% of the CO_2-slicing Tc reveals high clouds (Tc < 245 K) while their corresponding 11-μm brightness temperatures are much greater (~ 270 K). The differences between the warm 11-μm brightness temperatures and cold CO_2-slicing Tc indicate the presence of high transparent cirrus clouds.

The MODIS-retrieved cloud optical depths have very large values (> 10) for both high and low clouds as indicated by the cloud top temperatures of Tc < 250 K and Tc > 270 K, respectively. Without other information, the cold cloud-top temperatures associated with large optical depths would be interpreted as high thick clouds, while they are in fact low cloud overlapped by thin cirrus clouds. These two cloud configurations have completely different radiative effects and heating profiles. High thick clouds have a small net radiative forcing, but

large positive and negative forcing for the longwave and shortwave components, respectively. For thin cirrus clouds overlapping thick water clouds, the shortwave cooling dominates over the longwave warming so that the cloud system has a net strong cooling. Their heating profiles also differ considerably, leading to different thermodynamic and dynamic atmospheric conditions. A global survey of cloud vertical structure obtained from one year of sampled MODIS data indicates that cirrus-overlapping-low clouds account for about 40% of all low clouds and 50% of all high clouds (Chang and Li 2004). Such a high frequency of occurrence makes the single-layered assumption questionable if they are used for climate related studies.

3. Retrieval of the Optical Properties of Overlapping High and Low Clouds

3.1 Algorithm Development

After an overlapped cloud situation is identified, we assume a dual-layer cloud system comprised of a high cirrus cloud and a low water cloud layer in order to retrieve their individual properties. To illustrate the difference between single-layer and two-layer retrieval methods, we first demonstrate how the emissivity of the high cloud is estimated. For a single-layer overcast cirrus cloud, the satellite-observed radiance, $R(u)$, in an infrared window channel u (e.g., 11 μm) can be expressed as (e.g., Minnis et al. 1993a)

$$R(u) = e_{hc} R_{hc}(u) + (1 - e_{hc}) R_{\mathrm{clr}}(u), \qquad (1)$$

where $R_{\mathrm{clr}}(u)$ is the clear-sky sky radiance and $R_{hc}(u)$ is the equivalent blackbody radiance at the high-cloud temperature inferred from the MODIS CO_2-slicing-derived Tc. Rearranging Eq. (1), e_{hc} , the infrared cloud effective emissivity, is given by

$$e_{hc} = \frac{R(u) - R_{\mathrm{clr}}(u)}{R_{hc}(u) - R_{\mathrm{clr}}(u)}. \tag{2}$$

In the case of a cirrus cloud overlying a low cloud, the background clear-sky radiance $R_{\mathrm{clr}}(u)$ should be replaced by a radiance emitted from the low cloud and the surface, if the low cloud is not optically thick enough to completely block the surface emission. We can rewrite Eq.(1) as

$$R(u) = e_{hc} R_{hc}(u) + (1 - e_{hc}) R'(u), \tag{3}$$

$$R'(u) = e_{lc} R_{lc}(u) + (1 - e_{lc}) R_{\mathrm{clr}}(u), \tag{4}$$

where e_{lc} and $R_{lc}(u)$ are, respectively, the 11-μm effective emissivity and the equivalent blackbody radiance for the underlying low cloud. The high-cloud e_{hc} given in Eq.(2) is also modified accordingly as

$$e_{hc} = \frac{R(u) - R'(u)}{R_{hc}(u) - R'(u)}. \tag{5}$$

In general, the clear-sky surface temperature is warmer than the low cloud temperature, so $R_{clr}(u)$ is larger than $R'(u)$. For a cirrus-overlapping-low cloud, the cirrus cloud emissivity determined from Eq.(2) is thus overestimated relative to that given by Eq.(5).

For cirrus cloud, Eq.(5) is first used to determine the 11-μm e_{hc}. From the cirrus e_{hc}, one can derive its optical depth in the infrared region:

$$t_{IR} = -m \ln(1 - e_{hc}), \tag{6}$$

where m denotes the cosine of the satellite zenith angle.

The parameterization scheme developed by Minnis et al. (1993a) relates infrared emissivity to the visible optical depth (t_{VIS}) through an effective scattering ratio, x, given by

$$x = \frac{t_{VIS}}{t_{IR}}. \qquad (7)$$

In this study, we adopt the value of x = 2.13 that was derived for a cirrostratus hexagonal ice-crystal model (Takano and Liou 1989) and is equal to the mean value derived empirically from in-situ data by Minnis et al. (1990). The parameterization is also used by ISCCP for improving their ice cloud retrieval products (Rossow and Schiffer 1999). Although it may be argued that a more typical representation of ice clouds consists of randomly-oriented fractal crystals (Macke 1993; Mishchenko et al. 1996), Mishchenko et al. (1996) found that both hexagonal and fractal ice crystals produced similar results, except in the forward scattering directions; scattering in this direction is not encountered in satellite observations.

To determine the emitted radiance associated with the low cloud (i.e., $R'(u)$) in Eq.(4), the low-cloud equivalent blackbody radiance $R_{lc}(u)$ is determined from the mean low–cloud-top temperature inferred from neighboring low-cloud pixels. The low-cloud emissivity e_{lc} is calculated directly from the low-cloud t_{VIS}, which is retrieved from the visible channel through two-layer cloud modelling. Because high-cloud t_{VIS} is already determined from the infrared channel, the low-cloud t_{VIS} is thus retrieved as in a single-layer model, except the observed visible radiance is compared to that computed from a two-layer radiative transfer calculation with an input high-cloud t_{VIS}. As retrieval of the high-cloud t_{VIS} requires the knowledge of the underlying low-cloud t_{VIS} and vice-versa, retrieving the two requires an iterative process to obtain the best-fit between observations and models at both infrared and visible channels. This is automated as follows:

1. Assuming no low cloud is present, estimate an infrared optical depth for the cirrus cloud using Eq.(2).
2. Relate the infrared optical depth to the visible optical depth for the cirrus cloud using Eq.(6), i.e., $t_{VIS} = x t_{IR}$.
3. Retrieve the visible optical depth for the low cloud by comparing MODIS-observed visible radiance (0.86 μm for over water or 0.65 μm for over land) to modeled radiances from two-layer radiative transfer calculations. This step utilizes the cirrus t_{VIS} determined in the second step, the cirrus cloud-top altitude from the CO_2-slicing cloud-top pressure (Pc), and the low-cloud-top altitude from the neighboring low clouds.
4. Account for the low cloud effect using Eq.(4) and recalculate the cirrus t_{VIS} using Eqs.(5) and (7).
5. Repeat the second to fourth steps until the retrieved cirrus and low cloud optical depths converge to stable solutions. The iteration usually takes a couple of runs to converge because the underlying low clouds often have large optical depths that are nearly opaque at the 11-μm infrared channel. Therefore, the cirrus cloud emissivity calculated in Eq.(5) stabilizes quickly.

To speed up this process, lookup tables of two-layered cloud radiances are pre-calculated. In the visible radiative transfer calculations, an adding-doubling radiative transfer model described in Chang and Li (2002) is employed for the radiative transfer calculations, which assumes each layer to be plane-parallel and homogeneous. The upper cirrus layer is modeled using the fractal poly-crystals with a fixed effective radius of r_e = 30 μm, following the ISCCP ice-cloud model (Rossow and Schiffer 1999); this compares closely with observational data

(Minnis 1993b; Francis 1995; Descloitres et al. 1998). In particular, Descloitres et al. (1998) showed that the observed angular distributions of the visible reflectances from cirrus clouds agree within a few percent with the calculations based on the fractal –poly-crystal scattering phase functions. Cloud optical properties for the underlying low cloud layer are modeled using Mie theory and assumes spherical water droplets of a fixed effective radius of r_e = 10 μm (also following ISCCP). The refractive indices used in this study for the 0.65-μm channel are 1.308 + (1.365×10^{-8})i for ice and 1.332 + (1.672×10^{-8})i for water. For the 0.86-μm channel, the refractive indices are 1.304 + (2.106×10^{-7})i for ice and 1.329 + (3.290×10^{-7})i for water. Atmospheric transmittance and molecular scattering are calculated using MODTRAN-4 (Berk et al. 1999) and are based on the standard U.S. atmospheric temperature and humidity profiles. The surface albedos are determined using the bimonthly MODIS Filled Land Surface Albedo product and a constant of 0.05 is assumed for ocean. Uncertainties in surface albedo and atmospheric properties have little impact on the retrieval of cirrus cloud optical properties, but have more impact on the retrieved low-cloud optical depths.

The retrieval generates three output variables: cloud-top height (in pressure) , optical depths for both layers, and emissivity for the high cirrus clouds. From these retrievals and information on overlapping, each cloudy pixel can be classified into one of four categories, namely: 1) high, single-layer cirrus cloud with Pc < 500 mb and e_{hc} < 0.85; 2) high cirrus cloud with Pc < 500 mb and e_{hc} < 0.85, overlapping low cloud; 3) high thick cloud with Pc < 500 mb, but $e_{hc} \geq 0.85$; and 4) all other mid- and low clouds with Pc > 500 mb. Note that the overlapped retrieval is only applied for high cloud with e_{hc} < 0.85. For high thick clouds with $e_{hc} \geq 0.85$, the

retrieval of the underlying low-cloud properties are uncertain. Deep convective clouds like cumulonimbus usually accompany such high thick clouds.

3.2 Application Demonstration

Figure 3 illustrates the results obtained from the overlapped retrieval scheme that was applied to MODIS cloudy pixels with Tc < 250 K for the same cloudy scene as shown in Figs. 1 and 2 (the upper cluster of points in Fig. 2a). Note that the MODIS CO_2-slicing Tc is derived from data with a 5-km spatial resolution. The overlapped retrievals are applied to all 1-km MODIS pixels falling within each 5-km overcast scene (cloud cover fraction = 1.0). The retrieved t_{VIS} for the high cirrus clouds ranges from 0.01 to 1.5 with a mean value of 0.72. From the very low t_{VIS} of the cirrus clouds, one may conjecture that the optical depths of the low clouds would be similar to the single-layer cloud retrievals. This is not necessarily true and depends on whether the single-layer retrieval assumes an ice-phase or a water-phase cloud.

Figure 4 illustrates the effects of using a water or ice cloud model in the single-layer retrieval and the cirrus-over-water cloud model in the overlapped retrieval applied to the same data as in Fig. 3. The MODIS standard retrievals are also plotted. Because the MODIS retrievals use either an ice-cloud model or a water-cloud model, according to the phase determined by the MODIS algorithms (Platnick et al. 2003), three different single-layer retrievals are compared with the overlapped retrieval, which is the sum of high-cloud t_{VIS} plus low-cloud t_{VIS}. Figure 4 presents comparisons of t_{VIS} retrieved for overlapped low-level water clouds with MODIS single-layer retrievals of t_{VIS} assuming an ice-cloud model (Fig. 4a) and a water- cloud model (Fig. 4b.

To better isolate discrepancies caused by phase differences, also plotted in Fig. 4 are two additional single-layer retrievals for ice and water-phase clouds using the same effective particle

radius r_e = 10 μm, which is about the average of the mean r_e = 8.9 μm retrieved by MODIS for ice clouds (Fig. 4a) and 11.4 μm for water clouds (Fig. 4b). The optical depths retrieved using the ice model are more than 30% smaller than those retrieved using the water model. This is mainly due to the discrepancies in the scattering phase functions for ice crystals and water droplets (Mishchenko et al. 1996). The single-layer retrievals using the water-cloud model agree better with the overlapped retrievals because the cirrus clouds have very small t_{VIS}.

It is likely that the MODIS-retrieved r_e for single-layer ice clouds (mean r_e = 8.9 μm) are too small because the underlying water clouds enhance the near-infrared reflectance for the cirrus clouds, leading to smaller r_e retrievals. On the other hand, the MODIS-retrieved r_e for single-layer water clouds (mean r_e = 11.4 μm) were too large because the cirrus clouds attenuate the near-infrared reflectance for the water clouds, leading to larger r_e retrievals. There are also possibly reciprocal bias effects between the retrieved r_e and t_{VIS} due to cirrus-overlying-water clouds, which requires further investigation for verification.

For the cirrus t_{VIS} = 0.72 as shown in Fig. 3, the corresponding mean 11-μm e_{hc} is 0.285. Since these cirrus cloud properties are derived using Eq.(5), their sensitivities to uncertainties in $R_{hc}(u)$ and $R'(u)$ are examined. They essentially depend on the temperatures of the cirrus and low clouds, respectively. Figures 5a and 5b show changes in the mean e_{hc} and t_{VIS} to uncertainties (ΔTc) in the cirrus Tc and in the low-cloud Tc. The sensitivity tests are obtained independently for cirrus cloud and low clouds and the changes in mean cirrus e_{hc} and t_{VIS} are plotted as functions of ΔTc for either the cirrus or low cloud. The retrieved cirrus e_{hc} and t_{VIS} are much more sensitive to errors in low-cloud Tc than to errors in cirrus Tc. An error of ΔTc = ± 10 K in the high-cloud Tc results in a change of ± 0.1–0.2 in mean t_{VIS} but an error of ΔTc = ± 10 K in

the low-cloud Tc leads to a much larger change in mean t_{VIS} on the order of ~ ± 0.4–0.5. The point in the upper-right corner shows the retrieval where the low-cloud Tc is set equal to the surface temperature; it represents the error associated with the single-layer retrievals that assume no presence of low cloud. It leads to the largest bias errors in both e_{hc} (0.54) and t_{VIS} (1.53). The magnitude of these biases depends on the temperatures of the cirrus cloud, the low cloud and the background surface as well as on the t_{VIS} of the cirrus and low clouds.

Figure 6 shows the same sensitivity study as in Fig. 5, but for another cirrus-overlapping-low cloud case observed on April 18, 2001. On this day, the high-cloud Tc (~ 230 K), low-cloud Tc (~ 277 K) and surface temperature (~ 291 K) are similar to the high-cloud Tc (~ 232 K), low-cloud Tc (~ 278 K) and surface temperature (~ 293 K) on April 2 presented in Fig. 5. The low-cloud t_{VIS} (~ 5.5) on April 18 were on average much smaller than the t_{VIS} (~ 36) on April 2, leading to smaller e_{lc} and thus reducing the influence of the underlying low clouds. Hence, the uncertainties due to errors in low-cloud Tc shown in Fig. 6 are reduced by more than 30%. Moreover, because the contrast in the 11-μm radiances is increased between the cirrus cloud, $R_{hc}(u)$, and underlying background, $R'(u)$, the uncertainties due to errors in high-cloud Tc are also reduced significantly.

3.3 Comparisons of the retrieved cloud vertical structures with ground-based observations

The 35-GHz Millimeter-wave Cloud Profiling Radar (MMCR) deployed at the ARM SGP site can detect the simultaneous presence of thin cirrus clouds overlaying low clouds ; time-height cross-sections of the ground-based radar reflectivity factors during a four-hour span are shown in Figure 7a (for the April 2 case) and Figure 8a (for the April 18 case). The satellite

overpass time for the Terra/MODIS is approximately 1715 UTC. Figs. 7b and 8b show the frequency distributions of cloud-top heights (blue) derived from the ARM Active Remotely-Sensed Clouds Locations (ARSCL) value-added product (VAP) (Clothiaux et al. 2000) for the two days at the ARM SGP site. The ARSCL VAP retrieves cloud boundaries from a combination of MMCR and ground-based vertically pointing laser ceilometer, microwave radiometer, and micropulse lidar measurements. Also shown in Figs. 7b and 8b are the frequency distributions of cloud-top heights obtained from the overlapped retrieval scheme (red). Note that the cloud-top heights for the overlapped retrievals are based on a conversion from Pc to height (km). Pc values in pressure are also indicated (the right y-axis). In comparisons of the satellite retrievals and ground-based measurements, the overlapped retrievals are collected from a spatial domain over an area of about 1.5°-latitude × 1.5°-longitude centered at the ARM SGP site. The cloud-top heights from the ARSCL VAP are collected from 3-hour time series data within ± 1.5 hours of the MODIS overpass time. Despite the uncertainties that may be incurred by matching data sampled from two different platforms, both sets of measurements clearly show a similar two-layer cloud vertical structure consisting of a high cloud layer (> 6 km) and a low cloud layer (< 3.5 km). There are some differences in the frequency of occurrence in terms of cloud-top heights but this is mainly attributed to the fact that the ground point measurements are sampled every 10 seconds and the MODIS retrievals are sampled at a 5-km scale.

To put the differences in cloud vertical structure retrieved by different algorithms in context, we compare the Pc and t_{VIS} from the overlapped retrievals to those derived from the MODIS standard product (MOD06) and those derived from conventional retrievals like the bispectral visible-infrared method employed by the ISCCP. For the ISCCP-like visible-infrared bispectral method, we applied the retrievals to the 0.65-μm and 11-μm radiances observed by

MODIS. Figure 9 shows the frequency distributions of Pc and t_{VIS} from the three retrieval algorithms (overlapped on the left, MODIS product in the middle and ISCCP-like on the right). The different intervals are like those used in ISCCP (Rossow and Schiffer 1999). All overcast pixels falling within the area of 1.5°-latitude × 1.5°-longitude centered on the ARM Central Facility are processed by the three algorithms on the two days shown in Figs. 7 and 8. The results are compared separately for three overcast conditions found within the region: (a) cirrus overlying low clouds that account for about 45% of the clouds, (b) single-layer high clouds (both thin and thick) that account for about 5.2% of the clouds, and (c) single-layer low clouds that account for about 49.8% of the clouds.

Fig. 9a shows the differences for the cirrus-overlying-low-cloud cases. The CO_2-slicing technique employed by MODIS can accurately detect the high clouds, but none of the lower clouds beneath the high clouds are identified because a single-layer cloud is assumed in the MODIS cloud retrieval algorithm. It basically misidentifies the low thick clouds as high thick clouds. Use of the bispectral method simply cannot determine the altitudes of the overlapped cloud system. Instead, it misplaces them as mid-level clouds somewhere in between the high and low cloud altitudes.

For the single-layer high clouds (Fig. 9b), the two MODIS-based algorithms produce identical results, while higher cloud-top heights are retrieved by the ISCCP-like bispectral method. This is due to an overcorrection in the 11-μm Pc retrieval resulting from the small t_{VIS} retrieved at 0.63-μm. For single-layer low clouds (Fig. 9c), all three methods generate consistent results, as expected.

4. Conclusions

This study is motivated by surface and aircraft observations that showed a large probability of high cirrus clouds coexisting with low stratus clouds. Because cirrus clouds are optically thin and low stratus clouds are generally optically thicker, overlap of the two poses a major challenge for the detection of this cloud configuration and the retrieval of the associated optical properties by satellite remote sensing. To date, all operational satellite cloud retrieval algorithms employ radiative transfer models, which assume a single layer of cloud. Serious problems in the retrievals of several cloud properties, such as height, temperature, optical depth, and emissivity, can occur from using these algorithms due to the ubiquitous presence of cirrus-overlapping-low clouds. In this paper, a new satellite retrieval algorithm is proposed, which can cope with overlapping clouds. It is designed to take advantage of the wealth of information found in MODIS data. The algorithm can: 1) detect the presence of cirrus-overlapping-low clouds and 2) estimate their individual optical depths, cloud-top altitudes and emissivity for the upper thin clouds. It first utilizes 11-μm radiances to obtain a first guess of the cirrus cloud optical depth and utilizes 0.65-μm visible radiances to determine the low-cloud optical depth beneath the cirrus cloud. An iterative procedure then follows to adjust both the high and low cloud optical depths to match modeled radiances with MODIS-observed radiances at both the visible (0.65-μm) and infrared (11-μm) channels. The physical height of the cirrus cloud is determined by the CO_2-slicing technique, while the physical height of the low cloud is determined from neighboring MODIS pixels where single-layer low clouds are identified.

A sensitivity study shows that the retrieved cirrus cloud optical depth is not very sensitive to errors in cirrus cloud height and temperature, but very sensitive to errors in low-cloud temperature. The results presented in this study highlight both the importance of determining the

presence of overlapped clouds when applying any satellite retrieval algorithm and the uncertainties in satellite-retrieved cloud optical and microphysical properties estimated by the single-layered conventional algorithms. Large errors are found for cirrus-overlapping-water clouds if they are treated as single-layer water or ice clouds.

Preliminary comparisons are made of the cloud vertical structures retrieved from the new algorithm, the MODIS and ISCCP-like algorithms, and from the ground-based cloud radar and lidar deployed in north-central Oklahoma under the U.S. Department of Energy's Atmospheric Radiation Measurement Program. The comparisons show that the two-layer overlapping algorithm more correctly identifies cloud layers and that this algorithm more accurately estimates the cloud optical properties than the other two algorithms.

Acknowledgements

The authors are grateful to both the NASA Goddard Earth Sciences (GES) Distributed Active Archived Center (DAAC) for providing the MODIS data and the Atmospheric Radiation Measurement Program (ARM) for generating and distributing ground-based cloud data. Funding for this work was provided by the DOE grant DE-FG02-01ER63166 managed by Dr. Wanda Ferrell and a NASA grant NNG04GE79G managed by Dr. Hal Maring.

References

Ackerman, T. P., and G. Stokes, 2003: The Atmospheric Radiation Measurement Program. *Physics Today*, **56**, 38-45.

Baum, B. A., and B. A. Wielicki, 1994: Cirrus cloud retrieval using infrared sounding data: Multilevel cloud errors. *J. Appl. Meteor.*, **33**, 107-117.

Baum, B. A., T. Uttal, M. Poellot, T. P. Ackerman, J. M. Alvarez, J. Intrieri, D. O'C. Starr, J. Titlow, V. Tovinkere, and E. Clothiaux, 1995: Satellite remote sensing of multiple cloud layers, *J. Atmos. Sci.*, **52**, 4210-4230.

Baum, B. A., and J. D. Spinhirne, 2000: Remote Sensing of cloud properties using MODIS airborne simulator imagery during SUCCESS. 3. Cloud Overlap, *J. Geophys. Res.*, **105**, 11,793-11,804.

Berk, A., and Coauthors, 1999: MODTRAN4 v. 2.0 User's Manual. Air Force Geophysics Laboratory Tech. Rep. AFGL-TR-89-0122. 98 pp. [Available from Air Force Mat. Comm., Hanscomb AFB, Mass.]

Chang, F.-L., and Z. Li, 2002: Estimating the vertical variation of cloud droplet effective radius using multispectral near-infrared satellite measurements. *J. Geophys. Res.*, **107**, AAC 7 1-12.

Chang, F.-L., and Z. Li, 2004: A global climatology of single-layer and overlapped clouds and their optical properties developed using a new algorithm applied to Terra/MODIS data. Submitted.

Clothiaux, E. E., T. P. Ackerman, G. G. Mace, K. P. Moran, R. T. Marchand, M. Miller, and B. E. Martner, 2000: Objective determination of cloud heights and radar reflectivities using

a combination of active remote sensors at the ARM CART Sites. *J. Appl. Meteor.*, **39**, 645–665.

Coakley, J.A., Jr., and F. P. Bretherton, 1982: Cloud cover from high resolution scanner data: Detecting and allowing for partially filled fields of view. *J. Geophys. Res.*, **87**, 4917-4932.

Derber, J. C., D. F. Parrish, and S. J. Lord, 1991: The new global operational analysis system at the National Meteorological Center. *Weather Forecasting*, **6**, 538-547.

Descloitres, J. C., J. C. Buriez, F. Parol, and Y. Fouquart, 1998: POLDER observations of cloud bidirectional reflectances compared to a plane-parallel model using the International Satellite Cloud Climatology Project cloud phase functions. *J. Geophys. Res.*, **103**, 11,411-11,418.

Francis, P. N. 1995: Some aircraft observations of the scattering properties of ice crystals. *J. Atmos. Sci.*, **52**, 1142-1154.

Fye, F. K., 1978: The AFGWC automated cloud analysis model. Tech. Memo. 78-002, 97 pp. [Available from Air Force Global Weather Central, Offutt Air Force Base, NE, (ADA057176)]

Hahn, C. J., and Coauthors, 1982: Atlas of simultaneous occurrence of different cloud types over the ocean. NCAR tech. Note, TN241 + STR, 209 pp. [Available from National Center for Atmospheric Research, Boulder, CO 80307]

Hahn, C. J., S. G. Warren, J. London, R. M. Chervin, and R. Jenne, 1984: Atlas of simultaneous occurrence of different cloud types over land. NCAR Tech. Note TN-241 + STR, 216 pp. [Available from National Center for Atmospheric Research, Boulder, CO 80307]

Ho, S.-P., B. Lin, P. Minnis, and T.-F. Fan, 2003: Estimates of cloud vertical structure and water amount over tropical oceans using VIRS and TMI data, *J. Geophys. Res.*, **108**, AAC 10 1-16.

Jin, Y., W. B. Rossow, and D. P. Wylie, 1996: Comparison of the climatologies of high-level clouds from HIRS and ISCCP. *J. Climate*, **9**, 2850-2879.

King, M. D., W. P. Menzel, Y. J. Kaufman, D. Tanre, B. C. Gao, S. Platnick, S. A. Ackerman, L. A. Remer, R. Pincus, and P. A. Hubanks, 2003: Cloud and aerosol properties, precipitable water, and profiles of temperature and humidity from MODIS. *IEEE Trans. Geosci. Remote Sens.*, **41**, 442-458.

Lin, B., P. Minnis, B. Wielicki, D. R. Doelling, R. Palikonda, D. F. Young, and T. Uttal, 1998: Estimation of water cloud properties from satellite microwave, infrared and visible measurements in oceanic environment: 2. Results, *J. Geophys. Res.*, **103**, 3887-3905.

Mace, G. G., T. P. Ackerman, E. E. Clothiaux, and B. A. Albrecht, 1997: A study of composite cirrus morphology using data from a 94-GHz radar and correlations with temperature and large-scale vertical motion. *J. Geophys. Res.*, **102**, 13,581-13,593.

Mace, G. G., E. E. Clothiaux, T. A. Ackerman, 2001: The composite characteristics of cirrus clouds: Bulk properties revealed by one year of continuous cloud radar data, *J. Climate*, 1**4**, 2185-2203.

Macke, A., 1993: Scattering of light by polyhedral ice crystals. *Appl. Opt.*, **32**, 2780-2788.

Menzel, W. P., D. P. Wylie, and K. I. Strabala, 1992: Seasonal and diurnal changes in cirrus clouds as seen in four years of observations with the VAS. *J. Appl. Meteor.*, **31**, 370-385.

Menzel, W. P., B. A. Baum, K. I. Strabala, and R. A. Frey, 2002: Cloud top properties and cloud phase-Algorithm Theoretical Basis Document: ATBD-MOD-04, 61 pp. Available at http://modis-atmos.gsfc.nasa.gov/_docs/atbd_mod04.pdf.

Menzel, W. P., and L. E. Gumley, 2002: MODIS Atmospheric Profile Retrieval: Algorithm Theoretical Basis Document. ATBD-MOD-07, 36 pp. Available at http://modis-atmos.gsfc.nasa.gov/_docs/atbd_mod07.pdf.

Minnis, P., D. F. Young, K. Sassen, J. M. Alvarez, and C. J. Grund, 1990: The 27-28 October 1986 FIRE IFO Cirrus Case Study: Cirrus parameter relationships derived from satellite and lidar data. *Mon. Wea. Rev.*, **118**, 2402-2425.

Minnis, P., K.-N. Liou, and Y. Takano, 1993a: Inference of cirrus cloud properties using satellite-observed visible and infrared radiances. Part I: Parameterization of radiance field. *J. Atmos. Sci.*, **50**, 1279-1304.

Mishchenko, M. L., W. B. Rossow, A. Macke, and A. A. Lacis, 1996: Sensitivity of cirrus cloud albedo, bidirectional reflectance, and optical thickness retrieval accuracy to ice-particle shape. *J. Geophys. Res.*, **101**, 16,973-16,985.

Ou, S. C., K. N. Liou, and B. A. Baum, 1996: Detection of multilayer cirrus cloud systems using AVHRR data: Verification based on FIRE-II IFO composite measurements, *J. Appl. Meteorol.*, **35**, 178-191.

Platnick, S., M. D. King, S. A. Ackerman, W. P. Menzel, B. A. Baum, J. C. Riedi, and R. A. Frey, 2003: The MODIS cloud products: Algorithms and examples from Terra, *IEEE Trans. Geosci. Remote Sens.*, **41**, 459-473.

Rossow, W. B., and R. A. Schiffer, 1999: Advances in understanding clouds from ISCCP. *Bull. Amer. Meteor. Soc.*, **80**, 2261-2287.

Sheu, R.-S., J. A. Curry, and G. Liu, 1997: Vertical stratification of tropical cloud properties as determined from satellite, *J. Geophys. Res.*, **102**, 4231-4245.

Stephens, G. L., and coauthors, 2002: The CLOUDSAT mission and the A-Train, *Bull. Amer. Meteor. Soc.*, **83**, 1771-1790.

Takano, Y., and K.-N. Liou, 1989: Solar radiative transfer in cirrus clouds. Part I: Single scattering and optical properties of hexagonal ice crystal. *J. Atmos. Sci.*, **46**, 3-19.

Tian, L., and J. A. Curry, 1989: Cloud overlap statistics. *J. Geophys. Res.*, **94**, 9925-9935.

Wang, Z., and K. Sassen, 2002: Cirrus cloud microphysical property retrieval using lidar and radar measurements: I. Algorithm description and comparison with in situ data. *J. Appl. Meteor.*, **41**, 218-229.

Warren, S. G., C. J. Hahn, and J. London, 1985: Simultaneous occurrence of different cloud types. *J. Climate Appl. Meteor.*, **24**, 658-667.

Wylie, D. P., W. P. Menzel, H. M. Woolf, and K. I. Strabala, 1994: Four years of global cirrus cloud statistics using HIRS. *J. Climate*, **7**, 1972-1986.

Figure Captions

Fig. 1 The MODIS cloud imageries acquired on April 2, 2001 (1715 UTC) over an area of ~500 km × 300 km in north-central Oklahoma: a) 11-μm brightness temperature (K), b) CO_2-slicing-retrieved Tc (K), and c) 0.65-μm cloud optical depth. The square covers approximately $(50\ km)^2$ area centered at the ARM SGP Central Facility site.

Fig. 2 a) Comparison of MODIS retrieved CO_2-slicing Tc versus 11-μm brightness temperature. b) Comparison of MODIS retrieved CO_2-slicing Tc versus visible cloud optical depth for the boxed area shown in Fig. 1.

Fig. 3 The high-cloud and low-cloud Tc versus visible cloud optical depth as retrieved by the overlapped retrieval scheme for the data shown in Fig. 2b, but only for CO_2-slicing Tc less than 250 K.

Fig. 4 Comparisons of visible cloud optical depth from three single-layer retrievals (x-axis) and from the overlapped retrieval (y-axis) for MODIS-determined a) ice-phase cloud pixels and b) water-phase cloud pixels from boxed area shown in Fig. 1. Three single-layer retrievals are from the MODIS product (crosses), a water-droplet (r_e = 10 μm) cloud model (filled circles), and an ice-crystal (r_e = 10 μm) cloud model. Visible cloud optical depth is the sum of high and low clouds.

Fig. 5 Changes in the retrieved cirrus-cloud emissivity (a) and visible optical depth (b) due to changes in cirrus-cloud Tc (lines with open circles) or low-cloud Tc (lines with solid circles). The point on the upper-right corner is for the low-cloud Tc equal to the surface temperature.

Fig. 6 Same to Fig. 5, except for April 18, 2001 (1715 UTC).

Fig. 7 (a) Time-height cross section of the MMCR reflectivity measured on April 2, 2001 at ARM SGP site. (b) Cloud top heights/pressures from ARM-ARSCL VAP (blue) and MODIS overlapped retrievals (red).

Fig. 8 Same as in Fig. 7, except for April 18, 2001 (1715 UTC).

Fig. 9 Comparisons of three satellite retrieved frequency distributions of cloud top pressure (Pc) and optical depth (t_{VIS}) from the overlapped (left column), the MODIS-standard (middle column), and an ISCCP-like (right column) retrieval schemes. Comparisons are shown for three cloud types a) cirrus-overlapping-low cloud, b) single-layer high cloud, and c) single-layer low cloud, obtained over the ARM SGP site for an area of 1.5°-lat × 1.5°-lon on April 2 and 18, 2001 (UTC 1715).

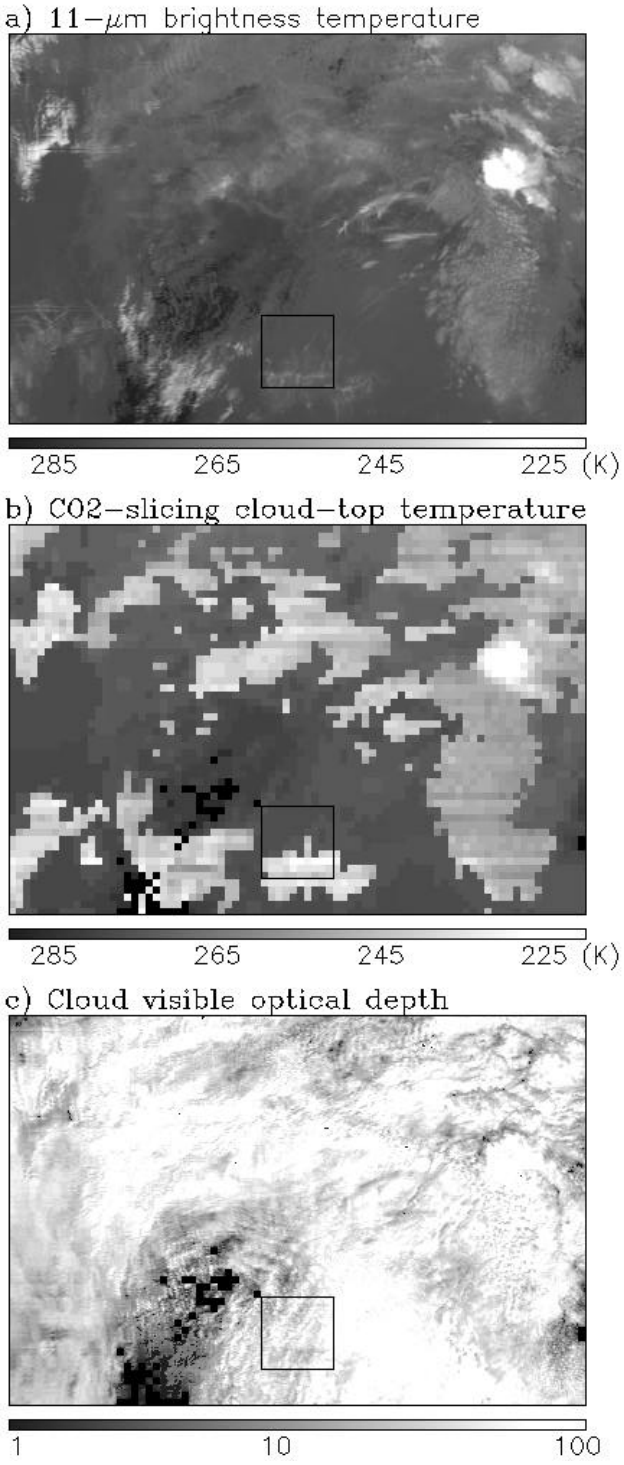

Fig. 1 MODIS images of a) 11-μm brightness temperature (K), b) CO_2-slicing-retrieved Tc (K), and c) 0.65-μm cloud optical depth for a geographical area of ~500 km × 300 km obtained on April 2, 2001 (1715 UTC) over north-central Oklahoma. The square box covers approximately 50 km^2 and is centered on the ARM SGP Central Facility site.

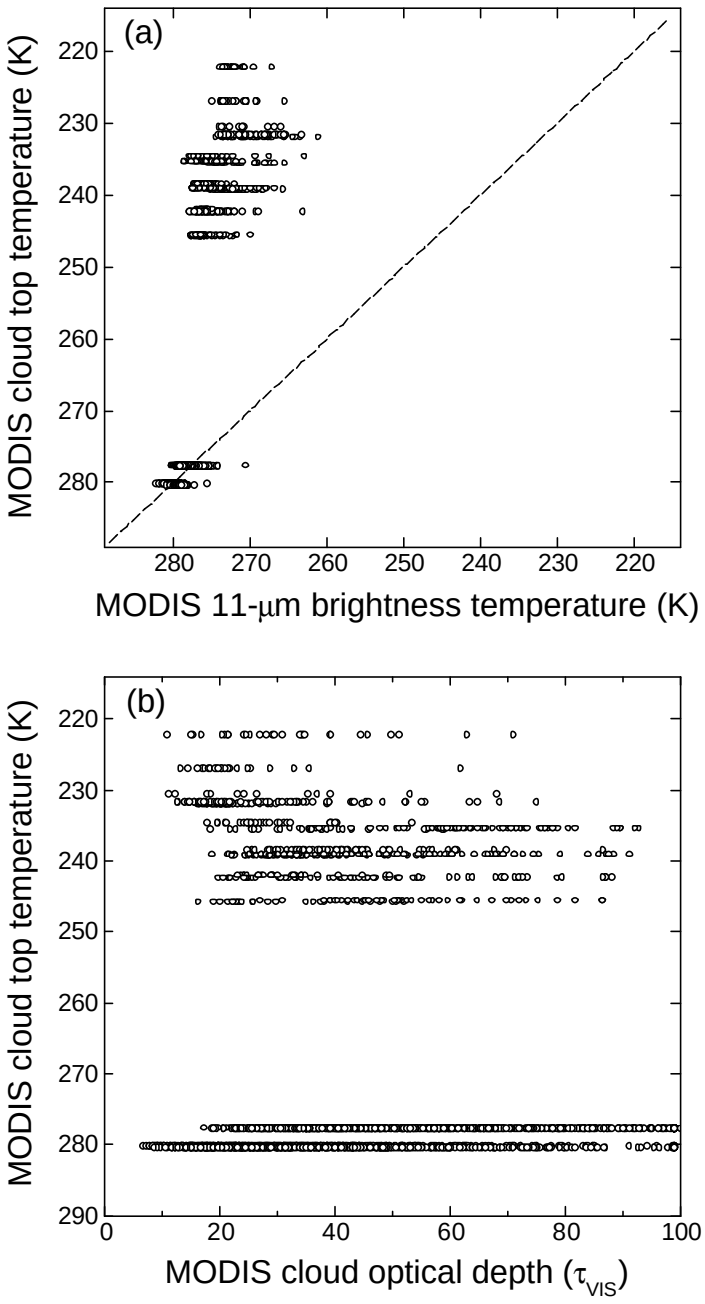

Fig. 2 a) MODIS-retrieved CO_2-slicing Tc as a function of observed 11-μm brightness temperature and b) MODIS-retrieved CO_2-slicing Tc as a function of t_{VIS} for the boxed area shown in Fig. 1.

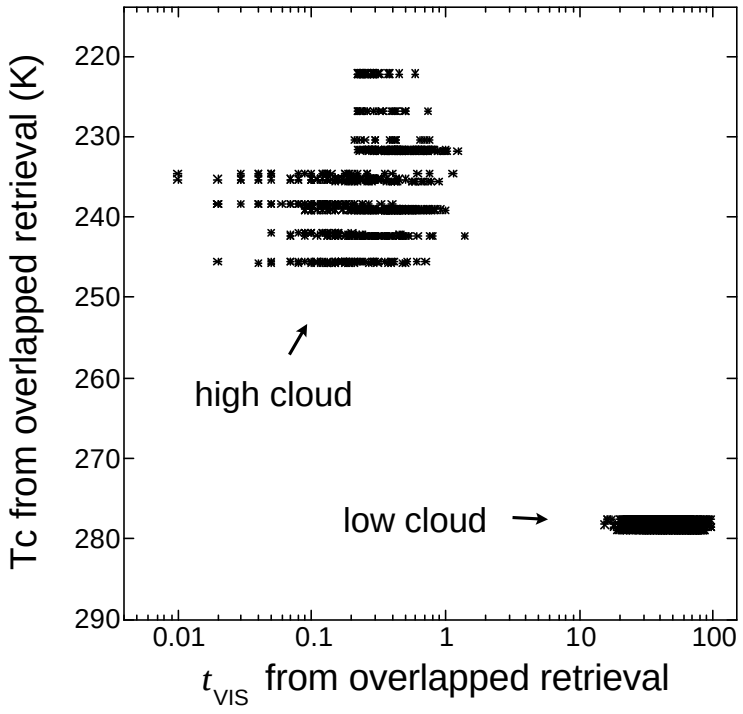

Fig. 3 The high-cloud and low-cloud Tc as a function of t_{VIS} retrieved by the overlapped retrieval scheme. Results are obtained for the data shown in Fig. 2b, but only for a CO_2-slicing Tc less than 250 K.

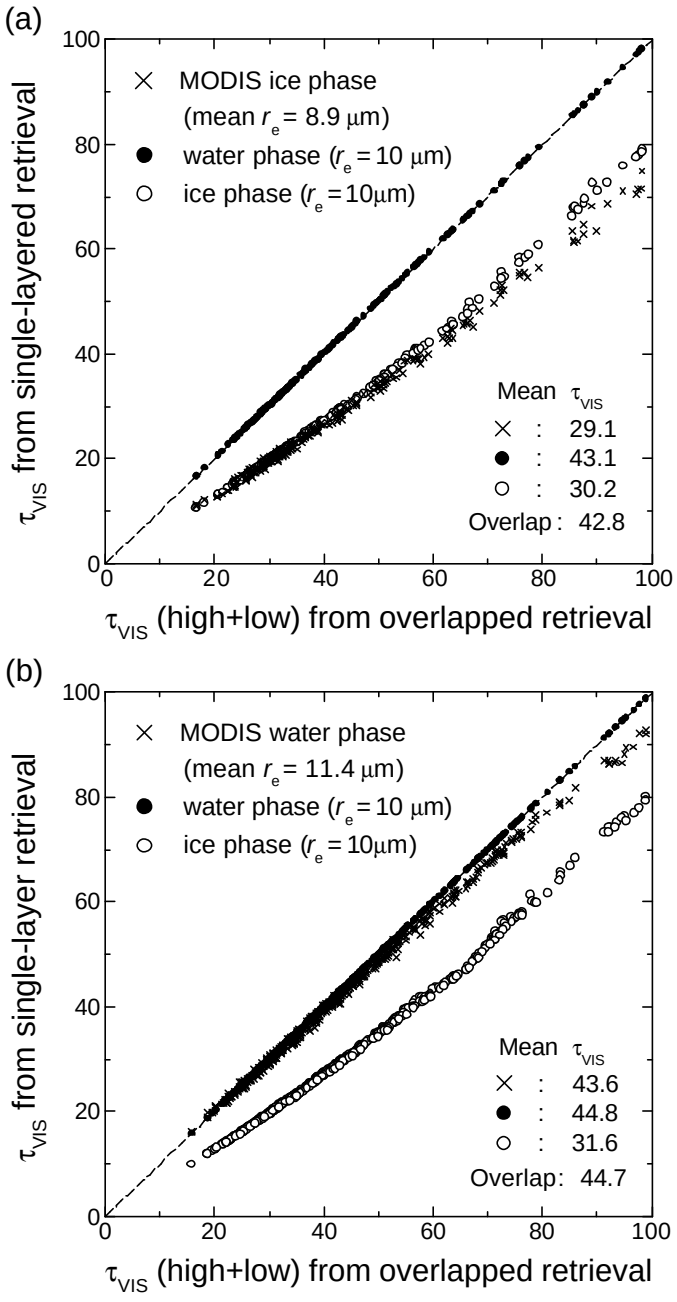

Fig. 4 Comparisons of t_{VIS} from three single-layered retrievals (y-axis) and from the overlapped retrieval (x-axis) for MODIS-determined a) ice-phase cloud pixels and b) water-phase cloud pixels. Results are obtained for the boxed area shown in Fig. 1. The three single-layered retrievals are from the MODIS product (crosses), a water-droplet (r_e = 10 μm) cloud model (filled circles), and an ice-crystal (r_e = 10 μm) cloud model. The t_{VIS} in the x-axis is the sum of both high-cloud t_{VIS} and low-cloud t_{VIS}.

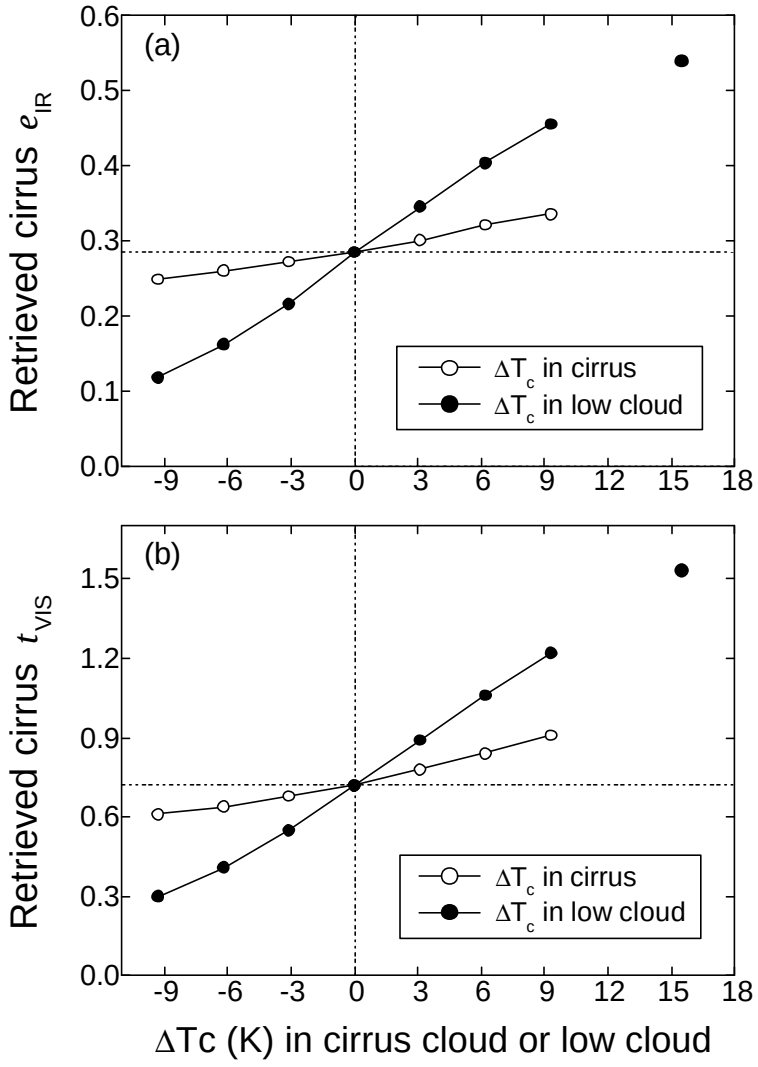

Fig. 5 Variations of retrieved cirrus e_{hc} (a) and t_{VIS} (b) with changes (ΔTc) in cirrus Tc (lines with open circles) and low-cloud Tc (lines with solid circles). The point in the upper-right corner is for a low-cloud Tc equal to the surface temperature.

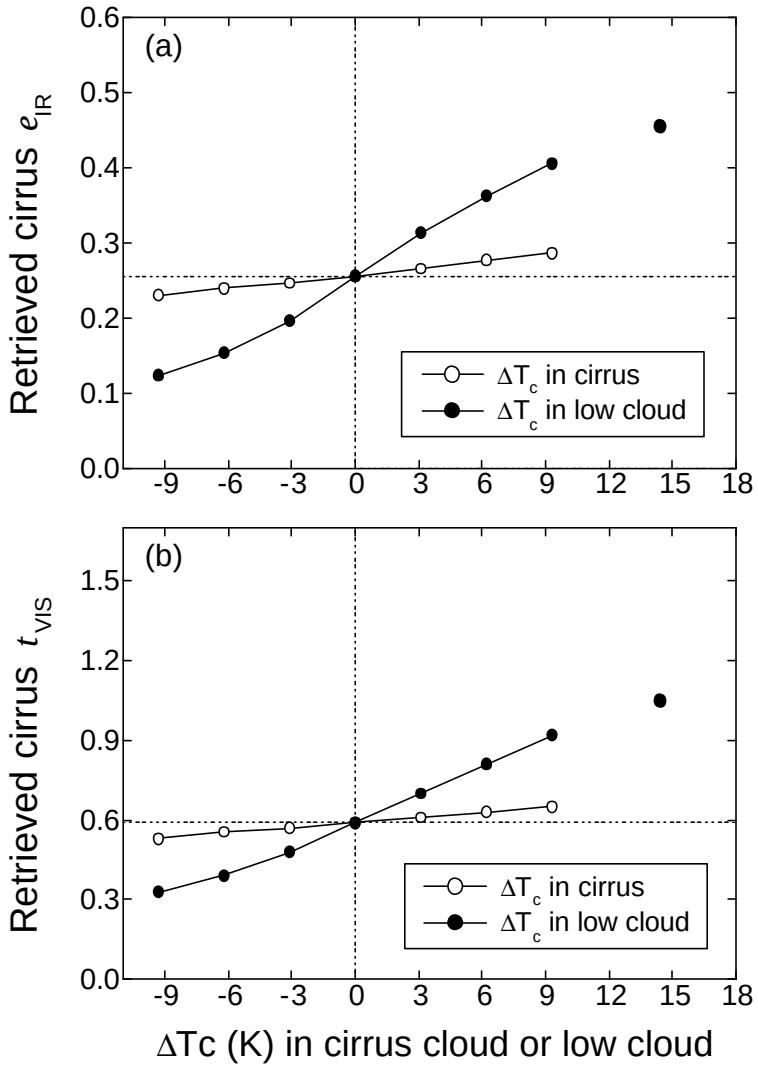

Fig. 6 Similar to Fig. 5, except for April 18, 2001 (1715 UTC).

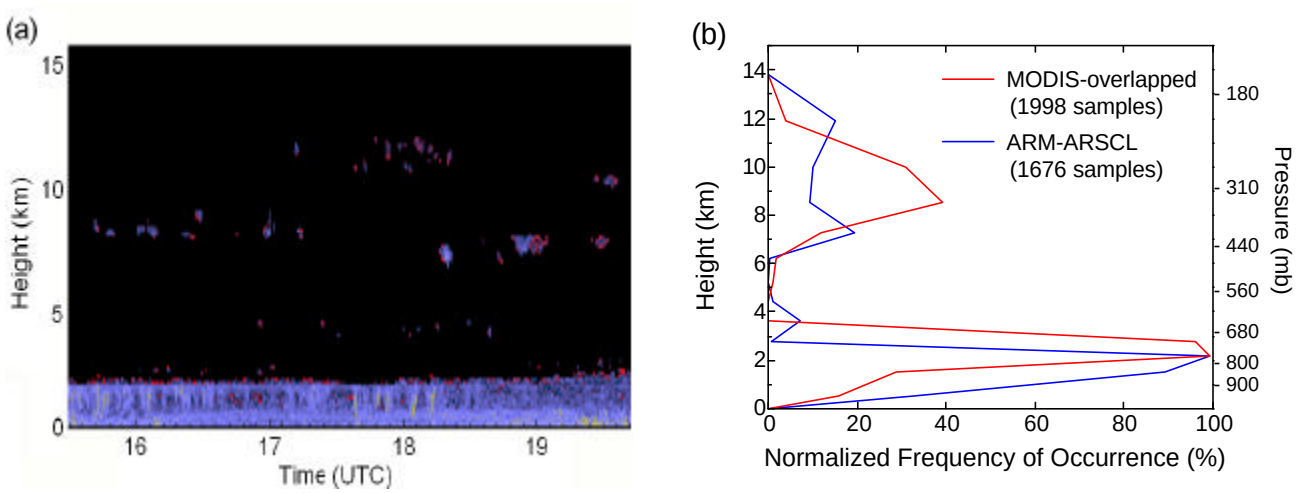

Fig. 7 (a) Time-height cross-section of the MMCR reflectivity measured on April 2, 2001 at the ARM SGP site. (b) Cloud top heights/pressures from the ARM ARSCL VAP (blue) and MODIS overlapped retrievals (red).

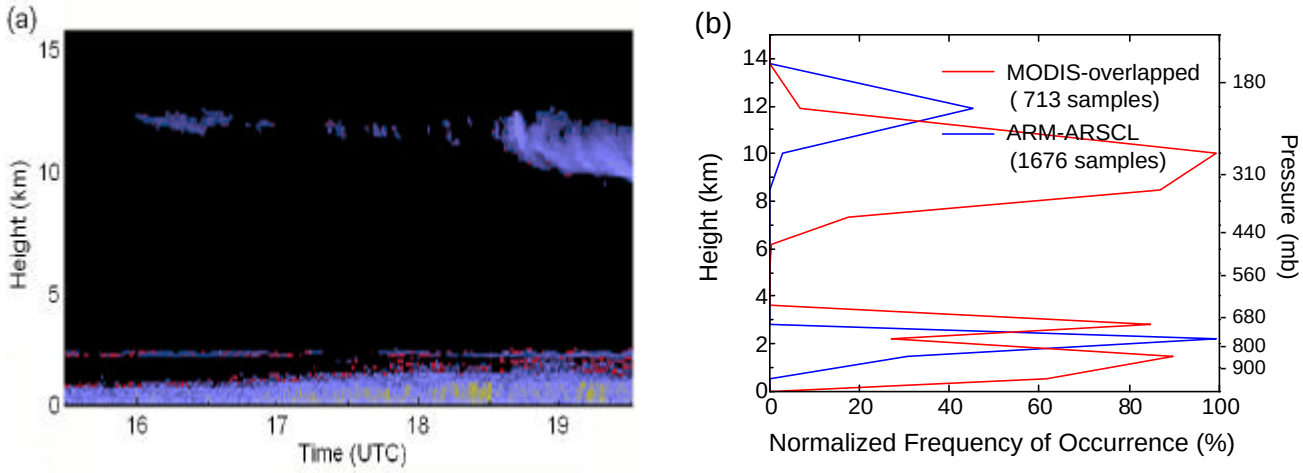

Fig. 8 Same as in Fig. 7, except for April 18, 2001 (1715 UTC).

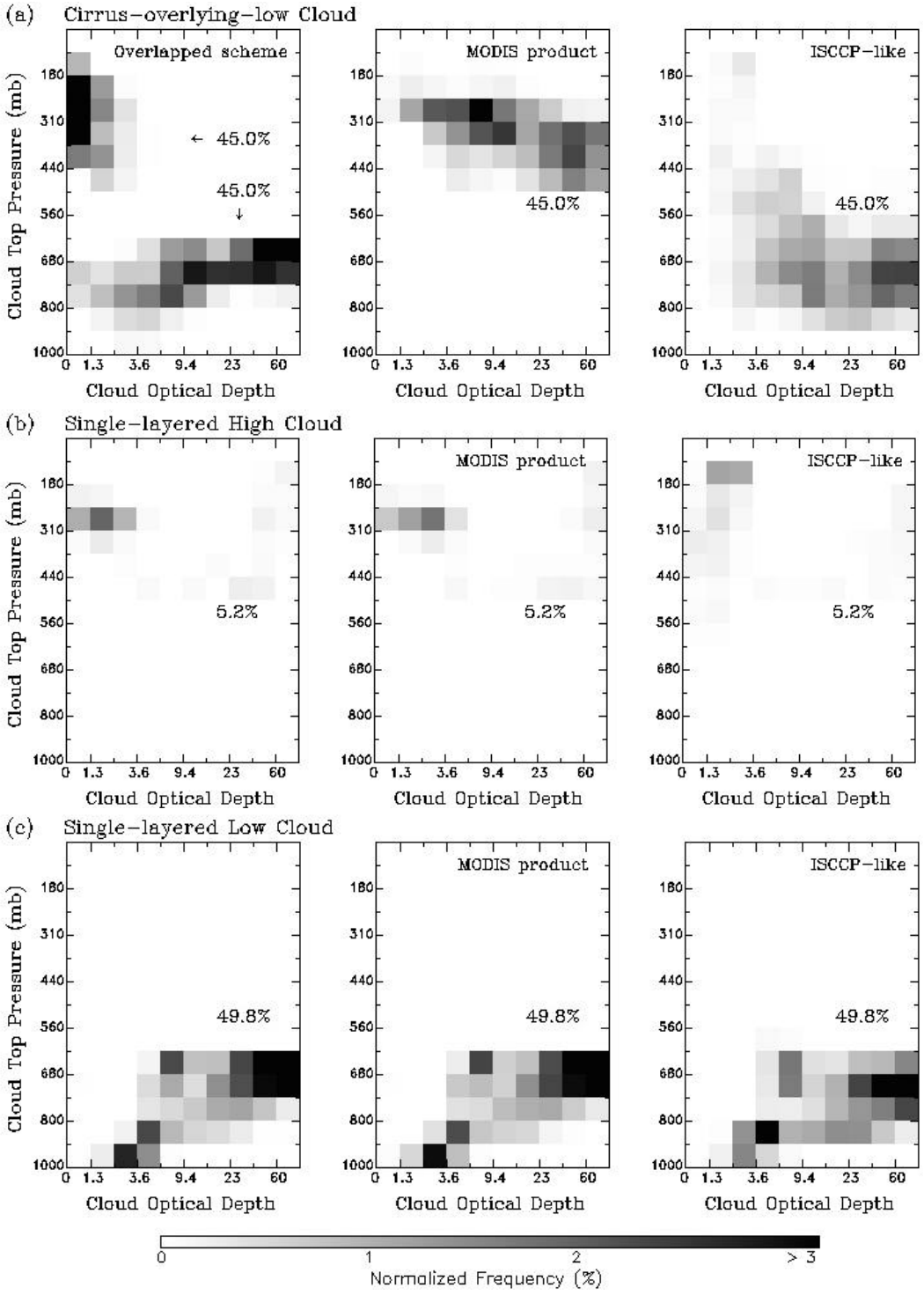

Fig. 9 Comparisons of three satellite-retrieved frequency distributions of cloud top pressure (Pc) and optical depth (t_{VIS}) from the overlapped (left column), the MODIS-standard (middle column), and an ISCCP-like (right column) retrieval schemes. Comparisons are shown for three cloud types a) cirrus-overlapping-low cloud, b) single-layer high cloud, and c) single-layered low cloud, obtained over an area of 1.5°-lat × 1.5°-lon centered on the ARM SGP site on April 2 and 18, 2001 (UTC 1715).